Tank Breakup Fragment Distribution Model

C. Johnson* and J. M. Taylor†
General Electric Company – TEMPO, Santa Barbara, Calif.

A joint normal probability distribution is derived for the position and velocity of fragments formed by the breakup of a booster tank upon atmospheric re-entry. The derivation proceeds from a knowledge of the statistical data on the fragment birth parameters of ballistic coefficient, altitude, and breakoff angle. The transformation of random variables from the birth parameters to the position and velocity coordinates is approximated using a first-order expansion about the mean birth parameters on the Allen and Eggers simplified dynamical equations of motion. The first term of the expansion is taken to be the mean of the distribution. The covariance is found by propagation of covariance using the expansion partial derivatives to form a partial derivative matrix relating birth parameter perturbations to position and velocity perturbations. The Allen and Eggers solution for the mean is improved to account for the round Earth and the effect of gravity on the velocity. The mean and covariance, which completely define the joint normal probability distribution, are parameterized by the tank lead edge altitude. The analytically derived mean and covariance matrix are compared to a statistical estimate that is based on a Monte Carlo sample population generated using a high-fidelity re-entry simulator.

Nomenclature

$\{a_i\}$	= position partial derivative set with respect to the birth parameters
$\{b_i\}$	= velocity magnitude partial derivative set with respect to the birth parameters
C,ρ	= scaling constants for atmospheric density model, density $=\rho \exp(-h/C)$
d	= distance along the breakoff trajectory
GM	= gravitational product
g	= acceleration of gravity
h	= altitude
K	= effective entry velocity
r	= range from center of the Earth
T_F	= time of flight
V	= velocity magnitude
X,Y,Z	= cloud coordinate set
β	= ballistic coefficient
γ	= flight path angle
θ	= breakoff angle
σ	= normal distribution standard deviation

Superscripts

$(\bar{\ })$	= mean value
$(\dot{\ })$	= derivative with respect to time
D	= daughter parameter
P	= parent parameter

Subscripts

AE	= value used in Allen and Eggers solution
C	= cloud coordinate set value
E	= conditions at atmospheric entry
LE	= conditions for lead edge fragment
x,y	= designates the cloud set coordinate
0	= conditions at fragment birth

Introduction

A NEED for reduced computer resources in ballistic missile defense simulations used for system technology radar software design and system performance evaluations led to a simplified approach of modeling booster tank breakup (TBU). An example TBU environment is illustrated in Fig. 1 for a radar tracking a single tank during atmospheric re-entry. The radar signal processor output is an amplitude observation for a range, angle, and range-rate sample. The "brute force" approach to modeling the TBU clutter is to map each fragment, along with a discrete representation for the fragment wake and the contiguous scatterer region through the radar simulator to the amplitude at the output of the signal processor. This can be a computational burden because of the large number of fragments produced in the TBU process. A Monte Carlo solution further increases the computational requirements because of the number of multiple realizations required for statistical confidence.

The simplified approach utilizes the fragment probability distributions in the radar coordinates in conjunction with the radar cross section and the time-delay, Doppler frequency ambiguity surface to determine those fragments and fragment wakes that can have amplitudes of sufficient magnitude to require high-fidelity simulation. The remaining fragments, fragment wakes, and contiguous scatters which represent the major portion of the TBU are simulated by modeling them in an aggregate fashion as an additional component to the normal receiver noise. The fragments are generated from a major booster tank piece called the "lead edge" fragment

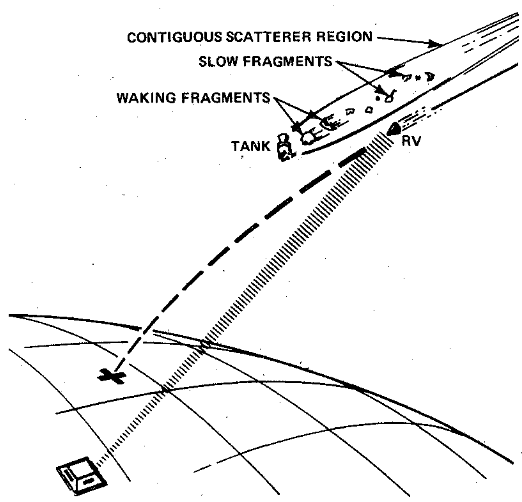

Fig. 1 TBU environment example.

Received Aug. 4, 1977; revision received Jan. 25, 1978.
Index category: LV/M Trajectories and Tracking Systems.
*System Analyst.
†System Analyst. Member AIAA.

which leads the fragment cloud because of its higher ballistic coefficient. The derivation of the fragment position and velocity probability distributions for any specified booster lead edge altitude is the major result of this paper.

An important byproduct of the Allen and Eggers[1] study into aerodynamic heating of ballistic missiles was their motion analysis. Generalized expressions were derived for the variation of speed and deceleration with altitude by assuming 1) that the gravity force is negligible compared to the aerodynamic drag, 2) an exponential atmospheric density variation with altitude, and 3) a constant ballistic coefficient. The use of the Allen and Eggers dynamical equations in an analytical probability analysis to determine position and velocity uncertainties caused by initial ballistic coefficient, altitude, and flight path angle uncertainties is new. The covariance analysis result, in particular, was found to be extremely accurate, using only the preceding assumptions to derive the partial derivatives. The expected value analysis is a solution to the entry trajectory using the mean values for the birth parameters. This mean value solution could readily be obtained by using a high-fidelity re-entry simulator.

An adequate total analytical solution is obtained by augmenting the Allen and Eggers solution to include the effect of gravity and provide an adjustment for a round Earth model. Moe[2] derived an approximation to ballistic entry trajectory that included the gravitational force in round Earth framework. A unified entry mechanics solution was developed by Loh[3-5] covering not only ballistic entry but joint lift-drag entry as well. An analytical solution similar to Loh's entry solution was also derived by Citron and Meir.[6] The fundamental difference between the preceding solutions and the solution given here is that the aerodynamic drag and gravity are considered separately and not jointly in solving the equations of motion.

Kepler's equations, which are used for the gravity-only solution, are superimposed on the Allen and Eggers solution giving a very simple entry trajectory approximation. This superimposed solution is limited to the entry region before significant trajectory bend. The more complicated joint analytical solutions also degrade in the bending portion of the trajectory, but they do not give a good qualitative result in that a 90 deg flight path angle is attained in the gravity-dominated region. This is not the case with the superimposed solution derived here, since only the linear trajectory region is modeled.

Dynamics and Birth Distributions

Allen and Eggers Dynamics

The generalized expression for the variation of speed with altitude for a ballistic entry body is given by

$$V = V_E \exp\left[\frac{-g\rho C \exp(-h/C)}{2\beta \sin\gamma_E}\right] \tag{1}$$

Inverting this expression gives the altitude, in terms of the velocity magnitude, as

$$h = C\ln\left[\frac{g\rho C}{2\beta \sin\gamma_E \ln(V_E/V)}\right] \tag{2}$$

The time of flight between two points on the trajectory, at which the velocity magnitudes are V_1 and V_2, can be derived[7] under the same assumptions as

$$T_F = \frac{C}{V_E \sin\gamma_E}\left\{\bar{E}i\ln\left(\frac{V_E}{V_2}\right) - \bar{E}i\ln\left(\frac{V_E}{V_1}\right)\right\} \tag{3}$$

where the exponential integral is defined by

$$\bar{E}i(x) \triangleq \int_{-\infty}^{x} e^z \frac{dz}{z} \tag{4}$$

These expressions for the velocity magnitude, altitude, and time of flight are fundamental to the development of the position and velocity probability density function given here.

TBU Birth Distributions

The random variables involved in the stochastic model for the flight of a fragment born from the booster tank lead edge are the birth altitude and ballistic coefficient and the flight path angle after birth. The joint distribution for these random variables, called the birth parameters, is postulated normal as follows

$$p(\beta_0) = N(\bar{\beta}_0, \sigma^2_{\beta_0}) \qquad p(h_0) = N(\bar{h}_0, \sigma^2_{h_0})$$
$$p(\theta_x) = N(0, \sigma^2_\theta) \qquad p(\theta_y) = N(0, \sigma^2_\theta) \tag{5}$$

The notation $N(\mu, \sigma^2)$ indicates a normal probability density function with mean μ and variance σ^2. The orthogonal breakoff angles θ_x and θ_y are relative to the velocity vector of the fragment, giving birth where θ_x is the in-plane angle and θ_y is the cross-plane angle. As noted in Eq. (5), the breakoff angle variances are assumed identical, $\sigma^2_{\theta_x} = \sigma^2_{\theta_y} = \sigma^2_\theta$. All four of the birth random variables are assumed to be statistically independent. The basis for the joint distribution mean and variance values is an empirical analysis of radar data collected on observed TBU. The means and variances are assumed known in this derivation.

Propagation of Covariance

The covariance analysis will consider both primary and secondary births. Primary fragmentation is where the birth event from the lead edge ends the fragmenting process for the born fragment. Secondary fragmentation occurs when a fragment born from the lead edge gives birth to another fragment. The fragment born from the lead edge is called the "parent" and its subsequent births are called "daughters."

Primary Fragmentation

The fragmentation geometry for primary birth is illustrated in Fig. 2. Depicted are the lead edge fragment and a born fragment at altitudes h_{LE} and h, respectively, with the birth event having occurred at altitude h_0. The fundamental coordinate system for the initial covariance solution is the shown X, Y, Z Cartesian set, called the cloud coordinate set, which has its origin at the projected impact point of the lead edge fragment. The straight-line entry trajectory for the lead edge is coincident with the Z axis and, when taken in conjunction, the X axis forms the azimuthal trajectory plane.

State Space Formulation

The position and velocity of the fragment in the cloud coordinates set are approximated, assuming small breakoff angles, as follows

$$X \approx \bar{d}\theta_x \tag{6}$$

$$Y \approx \bar{d}\theta_y \tag{7}$$

$$Z \approx h/\sin\gamma_E - \bar{d}\theta_x \cot\gamma_E \tag{8}$$

$$\dot{X} \approx \bar{V}\theta_x \tag{9}$$

$$\dot{Y} \approx \bar{V}\theta_y \tag{10}$$

$$\dot{Z} \approx -V \tag{11}$$

The distance d along the breakoff trajectory, shown in Fig. 2, is given by

$$d = (h_0 - h)/\sin(\gamma_E - \theta_x) \tag{12}$$

For a specified lead edge altitude, the fragment altitude and velocity have a dependence on the birth parameters denoted by $h=h(\beta_0,h_0,\theta_x)$ and $V=V(\beta_0,h_0,\theta_x)$. The velocity magnitude $\bar{V}$ and the altitude $\bar{h}$ are defined as $\bar{V}\triangleq V(\bar{\beta}_0,\bar{h}_0,0)$, $\bar{h}\triangleq h(\bar{\beta}_0,\bar{h}_0,0)$ and the distance $\bar{d}$ is given by

$$\bar{d}=(\bar{h}_0-\bar{h})/\sin\gamma_E \tag{13}$$

Expanding Z and $\dot{Z}$ in a first-order Taylor series around the mean birth parameters gives

$$\Delta Z=a_1\Delta\beta_0+a_2\Delta h_0+a_3\theta_x \tag{14}$$

$$\Delta\dot{Z}=b_1\Delta\beta_0+b_2\Delta h_0+b_3\theta_x \tag{15}$$

where

$$a_1=\frac{1}{\sin\gamma_E}\frac{\partial h}{\partial\bar{\beta}_0}(\bar{\beta}_0,\bar{h}_0,0) \tag{16}$$

$$a_2=\frac{1}{\sin\gamma_E}\frac{\partial h}{\partial\bar{h}_0}(\bar{\beta}_0,\bar{h}_0,0) \tag{17}$$

$$a_3=\frac{1}{\sin\gamma_E}\frac{\partial h}{\partial\theta}(\bar{\beta}_0,\bar{h}_0,\theta)\big|_{\theta=0}-\bar{d}\cot\gamma_E \tag{18}$$

$$b_1=-\frac{\partial V}{\partial\bar{\beta}_0}(\bar{\beta}_0,\bar{h}_0,0) \tag{19}$$

$$b_2=-\frac{\partial V}{\partial\bar{h}_0}(\bar{\beta}_0,\bar{h}_0,0) \tag{20}$$

$$b_3=-\frac{\partial V}{\partial\theta}(\bar{\beta}_0,\bar{h}_0,\theta)\big|_{\theta=0} \tag{21}$$

The covariance matrix for position and velocity in the cloud coordinate set simply becomes

$$S_C=M_CS_0M_C^T \tag{22}$$

where

$$S_0=\begin{bmatrix}\sigma^2_{\beta_0} & 0 & 0 & 0\\ 0 & \sigma^2_{h_0} & 0 & 0\\ 0 & 0 & \sigma^2_\theta & 0\\ 0 & 0 & 0 & \sigma^2_\theta\end{bmatrix} \tag{23}$$

$$M_C=\begin{bmatrix}0 & 0 & \bar{d} & 0\\ 0 & 0 & 0 & \bar{d}\\ a_1 & a_2 & a_3 & 0\\ 0 & 0 & \bar{V} & 0\\ 0 & 0 & 0 & \bar{V}\\ b_1 & b_2 & b_3 & 0\end{bmatrix} \tag{24}$$

The covariance matrix for position and velocity in the radar coordinate set S_R follows routinely by differentiating the transformation equations from the cloud coordinate set to the radar coordinate set and using them to propagate the covariance matrix S_C. This is a simple process for a flat Earth model and, hence, not carried out in this paper.

Altitude and Velocity Magnitude Partial Derivatives

The velocity of the fragment at birth follows from Eq. (1) as

$$V_0=V_E\exp\left[\frac{-g\rho C\exp(-h_0/C)}{2\beta_{\rm LE}\sin\gamma_E}\right] \tag{25}$$

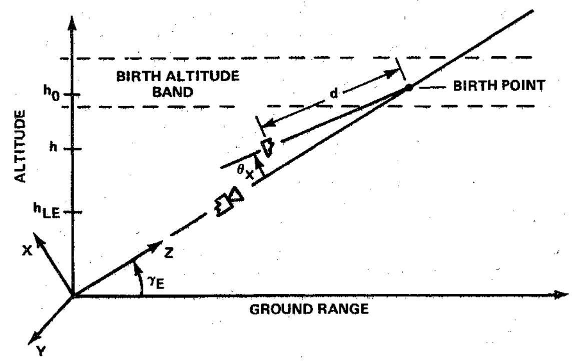

Fig. 2 Fragmentation geometry – primary birth.

An effective entry velocity for use in the dynamical equations describing the fragment trajectory after birth is found by solving Eq. (25) for V_E with $\beta_{\rm LE}$ and $\gamma_{\rm LE}$ replaced by β_0 and γ_0, respectively, giving

$$K_0=V_0\exp\left[\frac{g\rho C\exp(-h_0/C)}{2\beta_0\sin\gamma_0}\right] \tag{26}$$

where

$$\gamma_0=\gamma_E-\theta_x \tag{27}$$

The fragment altitude, in terms of the fragment velocity magnitude and the birth parameters, follows directly from Eq. (2) as

$$h=C\ln\left[\frac{g\rho C}{2\beta_0\sin\gamma_0\ln(K_0/V)}\right] \tag{28}$$

The lead edge time of flight from fragment birth to a specified lead edge altitude follows from Eq. (3) as

$$T_F=\frac{C}{V_E\sin\gamma_E}\left\{\bar{E}i\left[\ln\left(\frac{V_E}{V_{\rm LE}}\right)\right]-\bar{E}i\left[\ln\left(\frac{V_E}{V_0}\right)\right]\right\} \tag{29}$$

$$\triangleq m(h_0) \tag{30}$$

where the function $m(h_0)$ was introduced to indicate the dependence on the birth altitude. The lead edge altitude does not directly appear in the time-of-flight equation; however, the lead edge velocity magnitude $V_{\rm LE}$, in terms of lead edge altitude, is given by

$$V_{\rm LE}=V_E\exp\left[\frac{-g\rho C\exp(-h_{\rm LE}/C)}{2\beta_{\rm LE}\sin\gamma_E}\right] \tag{31}$$

The velocity of the fragment when the lead edge is at the specified altitude must satisfy the transcendental equation obtained by equating the lead edge time of flight to the fragment time of flight,

$$T_F=\frac{C}{K_0\sin\gamma_0}\left\{\bar{E}i\left[\ln\left(\frac{K_0}{V}\right)\right]-\bar{E}i\left[\ln\left(\frac{K_0}{V_0}\right)\right]\right\} \tag{32}$$

$$\triangleq f(V,\beta_0,h_0,\theta_x) \tag{33}$$

where the function $f(V,\beta_0,h_0,\theta_x)$ was introduced to indicate the dependence on the birth parameters. These derived quantities, when evaluated at the mean birth parameters $(\bar{\beta}_0,\bar{h}_0,0)$, are denoted by an overbar as follows:

$$\bar{V}_0=V_0(\bar{h}_0) \tag{34}$$

$$\bar{K}_0=K_0(\bar{\beta}_0,\bar{h}_0,0) \tag{35}$$

$$\bar{h}=h(\bar{V},\bar{\beta}_0,\bar{h}_0,0) \tag{36}$$

$$\bar{m}=m(\bar{h}_0) \tag{37}$$

$$\bar{f}=f(\bar{V},\bar{\beta},\bar{h}_0,0) \tag{38}$$

where the velocity $\bar{V}$ satisfies the transcendental equation $f(\bar{V},\bar{\beta}_0,\bar{h}_0,0)=m(\bar{h}_0)$.

To first-order the fragment altitude and velocity magnitude perturbations caused by the birth parameter perturbations about their mean values satisfy

$$\Delta h=\frac{\partial\bar{h}}{\partial\bar{V}}\Delta V+\frac{\partial\bar{h}}{\partial\bar{\beta}_0}\Delta\beta_0+\frac{\partial\bar{h}}{\partial\bar{h}_0}\Delta h_0+\frac{\partial h}{\partial\theta}\bigg|_{\theta=0}\theta_x \tag{39}$$

$$\frac{\partial\bar{m}}{\partial\bar{h}_0}\Delta h_0=\frac{\partial\bar{f}}{\partial\bar{V}}\Delta V+\frac{\partial\bar{f}}{\partial\bar{\beta}_0}\Delta\beta_0+\frac{\partial\bar{f}}{\partial\bar{h}_0}\Delta h_0+\frac{\partial f}{\partial\theta}\bigg|_{\theta=0}\theta_x \tag{40}$$

Solving for Δh and ΔV gives

$$\begin{aligned}\Delta h=&\left[\frac{\partial\bar{h}}{\partial\bar{\beta}_0}-\frac{\partial\bar{h}}{\partial\bar{V}}\left(\frac{\partial\bar{f}}{\partial\bar{V}}\right)^{-1}\frac{\partial\bar{f}}{\partial\bar{\beta}_0}\right]\Delta\beta_0\\&+\left[\frac{\partial\bar{h}}{\partial\bar{h}_0}-\frac{\partial\bar{h}}{\partial\bar{V}}\left(\frac{\partial\bar{f}}{\partial\bar{V}}\right)^{-1}\left(\frac{\partial\bar{f}}{\partial\bar{h}_0}-\frac{\partial\bar{m}}{\partial\bar{h}_0}\right)\right]\Delta h_0\\&+\left[\frac{\partial h}{\partial\theta}\bigg|_{\theta=0}-\frac{\partial\bar{h}}{\partial\bar{V}}\left(\frac{\partial\bar{f}}{\partial\bar{V}}\right)^{-1}\frac{\partial f}{\partial\theta}\bigg|_{\theta=0}\right]\theta_x\end{aligned} \tag{41}$$

$$\begin{aligned}\Delta V=&-\left(\frac{\partial\bar{f}}{\partial\bar{V}}\right)^{-1}\frac{\partial\bar{f}}{\partial\bar{\beta}_0}\Delta\beta_0-\left(\frac{\partial\bar{f}}{\partial\bar{V}}\right)^{-1}\left(\frac{\partial\bar{f}}{\partial\bar{h}_0}-\frac{\partial\bar{m}}{\partial\bar{h}_0}\right)\Delta h_0\\&-\left(\frac{\partial\bar{f}}{\partial\bar{V}}\right)^{-1}\frac{\partial f}{\partial\theta}\bigg|_{\theta=0}\theta_x\end{aligned} \tag{42}$$

Comparing Eqs. (41) and (42) with Eqs. (14) and (15), it is clear that

$$a_1=\frac{1}{\sin\gamma_E}\left[\frac{\partial\bar{h}}{\partial\bar{\beta}_0}-\frac{\partial\bar{h}}{\partial\bar{V}}\left(\frac{\partial\bar{f}}{\partial\bar{V}}\right)^{-1}\frac{\partial\bar{f}}{\partial\bar{\beta}_0}\right] \tag{43}$$

$$a_2=\frac{1}{\sin\gamma_E}\left[\frac{\partial\bar{h}}{\partial\bar{h}_0}-\frac{\partial\bar{h}}{\partial\bar{V}}\left(\frac{\partial\bar{f}}{\partial\bar{V}}\right)^{-1}\left(\frac{\partial\bar{f}}{\partial\bar{h}_0}-\frac{\partial\bar{m}}{\partial\bar{h}_0}\right)\right] \tag{44}$$

$$a_3=\frac{1}{\sin\gamma_E}\left[\frac{\partial h}{\partial\theta}\bigg|_{\theta=0}-\frac{\partial\bar{h}}{\partial\bar{V}}\left(\frac{\partial\bar{f}}{\partial\bar{V}}\right)^{-1}\frac{\partial f}{\partial\theta}\bigg|_{\theta=0}\right]-\bar{d}\cot\gamma_E \tag{45}$$

$$b_1=\left(\frac{\partial\bar{f}}{\partial\bar{V}}\right)^{-1}\frac{\partial\bar{f}}{\partial\bar{\beta}_0} \tag{46}$$

$$b_2=\left(\frac{\partial\bar{f}}{\partial\bar{V}}\right)^{-1}\left(\frac{\partial\bar{f}}{\partial\bar{h}_0}-\frac{\partial\bar{m}}{\partial\bar{h}_0}\right) \tag{47}$$

$$b_3=\left(\frac{\partial\bar{f}}{\partial\bar{V}}\right)^{-1}\frac{\partial f}{\partial\theta}\bigg|_{\theta=0} \tag{48}$$

The derivation of the intermediate partials of Eqs. (43-48) is straightforward with the results summarized in the Appendix.

Secondary Fragmentation

The fragmentation geometry for secondary birth is illustrated in Fig. 3. Depicted are the lead edge fragment with the parent and the daughter fragments on their respective breakoff trajectories. The lead edge fragment gave birth to the parent at h_0^P, with the parent, in turn, giving birth to a daughter at h_0^D.

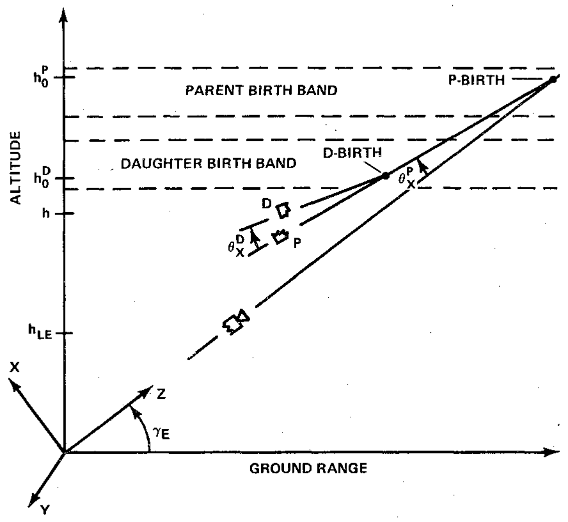

Fig. 3 Fragmentation geometry – secondary birth.

State Space Formulation

Assuming small breakoff angles, the position and velocity of the daughter fragment in the cloud coordinate set are approximated as

$$X\approx(\bar{d}^P+\bar{d}^D)\theta_x^P+\bar{d}^D\theta_x^D \tag{49}$$

$$Y\approx(\bar{d}^P+\bar{d}^D)\theta_y^P+\bar{d}^D\theta_y^D \tag{50}$$

$$Z\approx h/\sin\gamma_E-[(\bar{d}^P+\bar{d}^D)\theta_x^P+\bar{d}^D\theta_x^D]\cot\gamma_E \tag{51}$$

$$\dot{X}\approx\bar{V}(\theta_x^P+\theta_x^D) \tag{52}$$

$$\dot{Y}\approx\bar{V}(\theta_y^P+\theta_y^D) \tag{53}$$

$$\dot{Z}\approx-V \tag{54}$$

The distances along the trajectory from parent birth to daughter birth and from daughter birth to the daughter position evaluated using the mean birth parameters are given by

$$\bar{d}^P=(\bar{h}_0^P-\bar{h}_0^D)/\sin\gamma_E \tag{55}$$

$$\bar{d}^D=(\bar{h}_0^D-\bar{h})/\sin\gamma_E \tag{56}$$

As in primary fragmentation, the altitude and velocity magnitude have a dependence on the birth parameters, which are indicated by $h=h(\beta_0^P,h_0^P,\theta_x^P,\beta_0^D,h_0^D,\theta_x^D)$ and $V=V(\beta_0^P,h_0^P,\theta_x^P,\beta_0^D,h_0^D,\theta_x^D)$, respectively. Therefore,

$$\bar{h}\triangleq h(\bar{\beta}_0^P,\bar{h}_0^P,0,\bar{\beta}_0^D,\bar{h}_0^D,0) \tag{57}$$

$$\bar{V}\triangleq V(\bar{\beta}_0^P,\bar{h}_0^P,0,\bar{\beta}_0^D,\bar{h}_0^D,0) \tag{58}$$

Expanding Z and $\dot{Z}$ in a first-order Taylor series around the mean birth parameters gives

$$\Delta Z=a_1\Delta\beta_0^P+a_2\Delta h_0^P+a_3\theta_x^P+a_4\Delta\beta_0^D+a_5\Delta h_0^D+a_6\theta_x^D \tag{59}$$

$$\Delta\dot{Z}=b_1\Delta\beta_0^P+b_2\Delta h_0^P+b_3\theta_x^P+b_4\Delta\beta_0^D+b_5\Delta h_0^D+b_6\theta_x^D \tag{60}$$

where the sets $\{a_i\}$ and $\{b_i\}$ are the partial derivatives of h and V with respect to the birth parameters evaluated at their mean values. The covariance matrix for position and velocity in the cloud coordinate set simply becomes

$$S_C=M_C S_0 M_C^T \tag{61}$$

where

$$M_C = \begin{bmatrix} 0 & 0 & (\bar{d}^P+\bar{d}^D) & 0 & 0 & 0 & \bar{d}^D & 0 \\ 0 & 0 & 0 & (\bar{d}^P+\bar{d}^D) & 0 & 0 & 0 & \bar{d}^D \\ a_1 & a_2 & a_3 & 0 & a_4 & a_5 & a_6 & 0 \\ 0 & 0 & \bar{V} & 0 & 0 & 0 & \bar{V} & 0 \\ 0 & 0 & 0 & \bar{V} & 0 & 0 & 0 & \bar{V} \\ b_1 & b_2 & b_3 & 0 & b_4 & b_5 & b_6 & 0 \end{bmatrix}$$

and S_0 is the diagonal covariance matrix for the parent and daughter birth parameters as in Eq. (23).

Altitude and Velocity Magnitude Partial Derivatives

The velocity magnitudes for the parent and daughter at their respective birth altitudes follow from Eq. (1) as

$$V_0^P = V_E \exp\left[\frac{-g\rho C\exp(-h_0^P/C)}{2\beta_{\mathrm{LE}}\sin\gamma_E}\right] \tag{62}$$

$$V_0^D = K_0^P \exp\left[\frac{-g\rho C\exp(-h_0^D/C)}{2\beta_0^P\sin\gamma_0^P}\right] \tag{63}$$

where

$$K_0^P = V_0^P \exp\left[\frac{g\rho C\exp(-h_0^P/C)}{2\beta_0^P\sin\gamma_0^P}\right] \tag{64}$$

The daughter altitude, in terms of the daughter velocity magnitude and the birth parameters, follows from Eq. (2) as

$$h = C\ln\left[\frac{g\rho C}{2\beta_0^D\sin\gamma_0^D\ln(K_0^D/V)}\right] \tag{65}$$

where $\gamma_0^D = \gamma_E - \theta_x^P - \theta_x^D$ and the daughter effective entry velocity magnitude is given by

$$K_0^D = V_0^D \exp\left[\frac{g\rho C\exp(-h_0^D/C)}{2\beta_0^D\sin\gamma_0^D}\right] \tag{66}$$

It is clear that the daughter altitude expressed in this form depends on the velocity magnitude and birth parameters as denoted by $h=h(V,\beta_0^P,h_0^P,\theta_x^P,\beta_0^D,h_0^D,\theta_x^D)$. As before, with primary birth, the lead edge time of flight from parent birth to a specified lead edge altitude follows from Eq. (3) as

$$T_F = \frac{C}{V_E\sin\gamma_E}\left\{\bar{E}i\left[\ln\left(\frac{V_E}{V_{\mathrm{LE}}}\right)\right] - \bar{E}i\left[\ln\left(\frac{V_E}{V_0^P}\right)\right]\right\} \tag{67}$$

$$\triangleq m(h_0^P) \tag{68}$$

where the function $m(h_0^P)$ indicates the dependence on the parent birth altitude, and the lead edge velocity magnitude is given by

$$V_{\mathrm{LE}} = V_E \exp\left[\frac{-g\rho C\exp(-h_{\mathrm{LE}}/C)}{2\beta_{\mathrm{LE}}\sin\gamma_E}\right] \tag{69}$$

The velocity of the daughter when the lead edge is at a specified altitude must satisfy the transcendental equation obtained by equating the parent time of flight plus the daughter time of flight to the lead edge time of flight. Therefore,

$$T_F = T_F^P + T_F^D \tag{70}$$

where

$$T_F^P = \frac{C}{K_0^P\sin\gamma_0^P}\left\{\bar{E}i\left[\ln\left(\frac{K_0^P}{V_0^P}\right)\right] - \bar{E}i\left[\ln\left(\frac{K_0^P}{V_P^0}\right)\right]\right\} \tag{71}$$

$$\triangleq f_1(\beta_0^P,h_0^P,\gamma_0^P,h_0^D) \tag{72}$$

$$T_F^D = \frac{C}{K_0^D\sin\gamma_0^D}\left\{\bar{E}i\left[\ln\left(\frac{K_0^D}{V}\right)\right] - \bar{E}i\left[\ln\left(\frac{K_0^D}{V_0^D}\right)\right]\right\} \tag{73}$$

$$\triangleq f_2(V,\beta_0^P,h_0^P,\gamma_0^P,\beta_0^D,h_0^D,\gamma_0^D) \tag{74}$$

The functions $f_1(\beta_0^P, h_0^P, \gamma_0^P, h_0^D)$ and $f_2(V,\beta_0^P, h_0^P, \gamma_0^P, \beta_0^D, h_0^D, \gamma_0^D)$ were introduced to indicate the dependence on the birth parameters.

To first-order the altitude and velocity magnitude perturbations of the daughter caused by the birth parameter perturbations about their mean values satisfy

$$\Delta h = \frac{\partial\bar{h}}{\partial\bar{V}}\Delta V + \frac{\partial\bar{h}}{\partial\bar{\beta}_0^P}\Delta\beta_0^P + \frac{\partial\bar{h}}{\partial\bar{h}_0^P}\Delta h_0^P + \frac{\partial h}{\partial\theta^P}\bigg|_{\theta^P=0}\theta_x^P + \frac{\partial\bar{h}}{\partial\bar{\beta}_0^D}\Delta\beta_0^D + \frac{\partial\bar{h}}{\partial\bar{h}_0^D}\Delta h_0^D + \frac{\partial h}{\partial\theta^D}\bigg|_{\theta^D=0}\theta_x^D \tag{75}$$

$$\frac{\partial\bar{m}}{\partial\bar{h}_0^P}\Delta h_0^P = \frac{\partial\bar{f}_2}{\partial\bar{V}}\Delta V + \frac{\partial}{\partial\bar{\beta}_0^P}(\bar{f}_1+\bar{f}_2)\Delta\beta_0^P + \frac{\partial}{\partial\bar{h}_0^P}(\bar{f}_1+\bar{f}_2)\Delta h_0^P + \frac{\partial}{\partial\theta^P}(f_1+f_2)\big|_{\theta^P=0}\theta_x^P + \frac{\partial\bar{f}_2}{\partial\bar{\beta}_0^D}\Delta\beta_0^D + \frac{\partial}{\partial\bar{h}_0^D}(\bar{f}_1+\bar{f}_2)\Delta h_0^D + \frac{\partial f_2}{\partial\theta^D}\bigg|_{\theta^D=0}\theta_x^D \tag{76}$$

By solving Eqs. (75) and (76) for Δh and ΔV, it is clear that the partial derivatives indicated by the coefficients $\{a_i\}$ and $\{b_i\}$ follow from the coefficients of the birth parameter perturbations. Therefore,

$$a_1 = \frac{1}{\sin\gamma_E}\left(\frac{\partial\bar{h}}{\partial\bar{\beta}_0^P} - b_1\frac{\partial\bar{h}}{\partial\bar{V}}\right) \tag{77}$$

$$a_2 = \frac{1}{\sin\gamma_E}\left(\frac{\partial\bar{h}}{\partial\bar{h}_0^P} - b_2\frac{\partial\bar{h}}{\partial\bar{V}}\right) \tag{78}$$

$$a_3 = \frac{1}{\sin\gamma_E}\left(\frac{\partial h}{\partial\theta^P}\bigg|_{\theta^P=0} - b_3\frac{\partial\bar{h}}{\partial\bar{V}}\right) - (\bar{d}^D+\bar{d}^P)\cot\gamma_E \tag{79}$$

$$a_4 = \frac{1}{\sin\gamma_E}\left(\frac{\partial\bar{h}}{\partial\bar{\beta}_0^D} - b_4\frac{\partial\bar{h}}{\partial\bar{V}}\right) \tag{80}$$

$$a_5 = \frac{1}{\sin\gamma_E}\left(\frac{\partial\bar{h}}{\partial\bar{h}_0^D} - b_5\frac{\partial\bar{h}}{\partial\bar{V}}\right) \tag{81}$$

$$a_6 = \frac{1}{\sin\gamma_E}\left(\frac{\partial h}{\partial\theta^D}\bigg|_{\theta^D=0} - b_6\frac{\partial\bar{h}}{\partial\bar{V}}\right) - \bar{d}^D\cot\gamma_E \tag{82}$$

$$b_1 = \left(\frac{\partial\bar{f}_2}{\partial\bar{V}}\right)^{-1}\frac{\partial(\bar{f}_1+\bar{f}_2)}{\partial\bar{\beta}_0^P} \tag{83}$$

$$b_2 = \left(\frac{\partial\bar{f}_2}{\partial\bar{V}}\right)^{-1}\left[\frac{\partial(\bar{f}_1+\bar{f}_2)}{\partial\bar{h}_0^P} - \frac{\partial\bar{m}}{\partial\bar{h}_0^P}\right] \tag{84}$$

$$b_3 = \left(\frac{\partial\bar{f}_2}{\partial\bar{V}}\right)^{-1}\frac{\partial(f_1+f_2)}{\partial\theta^P}\bigg|_{\theta^P=0} \tag{85}$$

$$b_4=\left(\frac{\partial\bar{f}_2}{\partial\bar{V}}\right)^{-1}\frac{\partial\bar{f}_2}{\partial\beta_0^D} \tag{86}$$

$$b_5=\left(\frac{\partial\bar{f}_2}{\partial\bar{V}}\right)^{-1}\frac{\partial(\bar{f}_1+\bar{f}_2)}{\partial\bar{h}^D} \tag{87}$$

$$b_6=\left(\frac{\partial\bar{f}_2}{\partial\bar{V}}\right)^{-1}\frac{\partial f_2}{\partial\theta^D}\bigg|_{\theta^D=0} \tag{88}$$

The intermediate partial derivatives of Eqs. (77-88) are summarized in the Appendix.

Improved Allen and Eggers Solution

Round Earth Improvement

The Allen and Eggers motion analysis is generally placed in a flat Earth setting with the ground range from impact being related to the altitude as $GR=h/\tan\gamma$. Initial use of this flat Earth formulation showed that for long-range trajectories an improved trajectory model was required to account for the Earth's curvature. Examination of trajectory contours, generated by numerically integrating the complete dynamics, shows that for high-β bodies the altitude is nearly linear with the round Earth ground range.[8] Of course, as β decreases, the ground range altitude contours begin to curve over in the lower-altitude regions. However, the linearity was found to hold for the altitude interval and β class involved in modeling TBU. Based on this observation, the Allen and Eggers solution was placed in an altitude-round Earth ground range coordinate set. This improved coordinate set is illustrated in Fig. 4a. The flight path angle to be used in the solution is fixed by the linear part of the contour as denoted by γ_{AE}. The round Earth ground range, GR, follows from the altitude and flight path angle as

$$GR=h/\tan\gamma_{AE} \tag{89}$$

The GR,h coordinates of a body placed in the round Earth geometry are illustrated in Fig. 4b. The slope dh/dGR at any point on the actual trajectory is given by

$$\frac{dh}{dGR}=\frac{(r_e+h)}{r_e}\tan\gamma \tag{90}$$

The flight path angle γ_{AE} is found by equating its tangent to

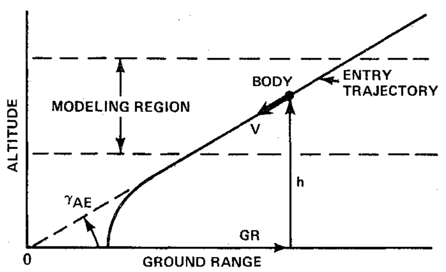

Fig. 4a Allen and Eggers improved dynamics coordinate set.

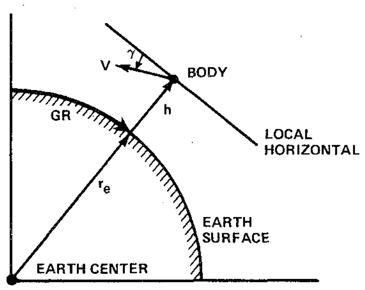

Fig. 4b Round Earth geometry.

the slope dh/dGR at a median point in the modeling region since $dh/dGR\approx$const. Therefore,

$$\tan\gamma_{AE}=\frac{(r_e+h)}{r_e}\tan\gamma\,|_{h=h_M} \tag{91}$$

where h_M is the designated altitude in the modeling region.

Velocity Improvement

The flight path angle given by the Kepler solution to the motion of a ballistic body, subject only to an inverse square law gravitational field, agrees closely in the modeling region to the flight path determined from a numerically integrated trajectory having both drag and gravity effects. Since this is the case, the flight path angle γ_{AE} can be determined by an analytical model by replacing the actual flight angle γ by the Keplerian flight path angle as

$$\tan\gamma_{AE}=\frac{(r_e+h)}{r_e}\tan\gamma_K\,|_{h=h_M} \tag{92}$$

where γ_K denotes the Keplerian angle. Furthermore, the actual flight path angle, as a function of the altitude, can be approximated as

$$\tan\gamma\approx\frac{r_e}{(r_e+h)}\tan\gamma_{AE} \tag{93}$$

once the flight path angle γ_{AE} has been established. Equations (92) and (93) taken together form a complete analytical model for the flight path angle.

Gravity has a noticeable effect in the early entry regions where the drag is small; i.e., velocity magnitude increases as altitude decreases. The velocity magnitude adjustment for gravity is also facilitated by Kepler's equations of motion. The expression for the velocity magnitude improvement is given by

$$\Delta V=(h-h_E)\frac{dV}{dr}\bigg|_{h=h_E} \tag{94}$$

where h_E denotes the entry altitude and

$$\frac{dV}{dr}=-\frac{GM}{Vr^2} \tag{95}$$

The oscillations in the atmospheric density profile about a single exponential model fit also cause deviations in the velocity magnitude. A reduction of this component of velocity variation over the modeling region is obtained by defining the exponential model over three altitude intervals, changing the model coefficients as the trajectory moves through each interval.

Model Verification

Table 1 compares the analytical solution for the mean and the covariance matrix to a high-fidelity trajectory simulator solution having complete drag, gravity, and round Earth entry dynamics. The simulator solution standard deviations and correlation coefficients are statistical estimates based on a sample population generated from 5000 joint realizations of the birth process. The simulator-solution Cartesian coordinate set used to display the covariance matrix comparisons was selected so that it nearly aligns with the flat Earth cloud coordinate set. The origin of the coordinate set was taken at the mean fragment position in order that the position realizations correspond to perturbations about the mean value solution. The Z axis points back along the trajectory at the angle $\bar{\gamma}$, Eq. (93), with the local vertical. The Y axis is taken normal to the mean trajectory plane with the X axis completing the orthogonal set. The comparison is made for both

Table 1 Mean value and covariance matrix comparisons

Normal Probability Density Elements	Primary Fragmentation $\bar{\beta}_0$ (lb/ft^2) 15	Primary Fragmentation $\bar{\beta}_0$ (lb/ft^2) 5	Secondary Fragmentation $\bar{\beta}_0^D$ (lb/ft^2) 15	Secondary Fragmentation $\bar{\beta}_0^D$ (lb/ft^2) 5
$\bar{h}$ (kft)	93.551[a] 93.487[b]	102.659 102.568	90.489 90.453	93.517 93.478
$\overline{GR}$ (kft)	131.785 131.760	144.616 144.564	127.470 127.470	131.736 131.712
$\bar{V}$ (kft/s)	5.914 5.928	3.035 3.042	6.163 6.200	3.173 3.200
$\bar{\gamma}$ (deg)	35.250 35.697	35.238 36.163	35.254 35.626	35.250 35.837
σ_x (kft)	0.797 0.803	0.523 0.509	0.935 0.933	0.822 0.819
σ_y (kft)	0.797 0.780	0.523 0.523	0.935 0.925	0.822 0.810
σ_z (kft)	2.399 2.485	5.840 6.331	1.483 1.518	3.306 3.493
$\sigma_{\dot{x}}$ (kft/s)	0.103 0.103	0.053 0.052	0.152 0.153	0.078 0.083
$\sigma_{\dot{y}}$ (kft/s)	0.103 0.100	0.053 0.054	0.152 0.152	0.078 0.082
$\sigma_{\dot{z}}$ (kft/s)	0.449 0.447	0.823 0.818	0.465 0.471	0.942 0.968
$\rho_{x\dot{x}}$	1.000 0.996	1.000 0.994	0.890 0.878	0.855 0.824
$\rho_{y\dot{y}}$	1.000 0.996	1.000 0.994	0.890 0.883	0.855 0.828
$\rho_{z\dot{z}}$	0.754 0.759	0.872 0.881	0.545 0.548	0.733 0.755
ρ_{xz}	-0.084 -0.092	-0.021 -0.026	-0.234 -0.231	-0.178 -0.152
$\rho_{x\dot{z}}$	-0.179 -0.188	-0.040 -0.041	-0.269 -0.251	-0.101 -0.083

[a] Analytical solution values.
[b] Complete trajectory simulation values.

Table 2 Lead edge trajectory comparison

h (kft)	β_{LE} = 100 lb/ft^2 V (kft/s)	β_{LE} = 100 lb/ft^2 GR (kft)	β_{LE} = 100 lb/ft^2 γ (deg)	β_{LE} = 30 lb/ft^2 V (kft/s)	β_{LE} = 30 lb/ft^2 GR (kft)	β_{LE} = 30 lb/ft^2 γ (deg)
200	22.463[a] 22.462[b]	281.246 281.235	35.113 35.123	22.287 22.287	281.246 281.237	35.113 35.124
180	22.388 22.392	253.073 253.071	35.139 35.148	21.975 21.983	252.073 253.077	35.139 35.152
160	22.203 22.217	224.899 224.907	35.164 35.174	21.314 21.338	224.899 224.918	35.164 35.184
140	21.797 21.807	196.726 196.746	35.190 35.203	19.984 19.995	196.726 196.773	35.190 35.227
120	20.834 20.826	168.552 168.589	35.216 35.236	17.143 17.108	168.555 168.659	35.216 35.297
110	19.913 19.908	154.466 154.518	35.228 35.262	14.725 14.705	154.472 154.631	35.228 35.360
100	18.513 18.508	140.378 140.452	35.241 35.293	11.533 11.529	140.378 140.628	35.241 35.472
80	13.634 13.646	112.207 112.373	35.267 35.414	4.181 4.249	112.205 113.004	35.267 36.445
60	6.220 6.181	84.032 84.524	35.293 35.932	0.399 0.652	84.031 90.645	35.293 57.544
50	2.903 2.881	69.945 71.025	35.306 37.343	0.146 0.433	69.944 87.042	35.306 81.090

[a] Improved Allen and Eggers solution values.
[b] Complete trajectory simulation values.

Table 3 RV trajectory comparison ($\beta = 1500$ lb/ft^2)

h (kft)	γ_E = 35 deg V (kft/s)	γ_E = 35 deg GR (kft)	γ_E = 35 deg γ (deg)	γ_E = 25 deg V (kft/s)	γ_E = 25 deg GR (kft)	γ_E = 25 deg γ (deg)
200	22.535[a] 22.535[b]	281.746 281.735	35.113 35.122	22.533 22.533	420.097 420.097	25.247 25.183
180	22.556 22.556	253.572 253.570	35.139 35.146	22.551 22.552	378.087 377.978	25.268 25.219
160	22.569 22.570	225.399 225.403	35.164 35.170	22.560 22.561	336.078 335.889	25.289 25.255
140	22.567 22.568	197.225 197.234	35.190 35.194	22.548 22.549	294.069 293.828	25.310 25.291
120	22.525 22.525	169.052 169.064	35.216 35.218	22.482 22.481	252.060 251.797	25.331 25.327
110	22.470 22.470	154.965 154.978	35.228 35.231	22.403 22.402	231.055 230.792	25.346 25.342
100	22.374 22.374	140.878 140.892	35.241 35.243	22.269 22.268	210.051 209.796	25.352 25.366
80	21.947 21.948	112.706 112.722	35.267 35.271	21.690 21.690	168.042 167.832	25.374 25.410
60	20.848 20.828	84.531 84.556	35.293 35.306	20.226 20.207	126.031 125.922	25.395 25.468
40	18.219 18.134	56.357 56.410	35.319 35.363	16.868 16.772	84.030 84.127	25.416 25.575

[a] Improved Allen and Eggers solution values.
[b] Complete trajectory simulation values.

primary and secondary fragmentation examples and each considers two cases for the fragment mean birth ballistic coefficient. The lead edge fragment is fixed at an altitude of $h_{LE} = 80$ kft, having flown down from atmospheric entry ($h_E = 300$ kft, $V_E = 22.4$ kft/s, and $\gamma_E = 35$ deg) with a ballistic coefficient of $\beta_{LE} = 100$ lb/ft^2. The mean birth parameters for the example cases were selected as follows:

Primary fragmentation

$$\bar{h}_0 = 120 \text{ kft} \qquad \bar{\beta}_0 = 15 \text{ and } 5 \text{ lb/ft}^2$$

Secondary fragmentation

Parent

$$\bar{h}_0^P = 120 \text{ kft} \qquad \bar{\beta}_0^P = 25 \text{ lb/ft}^2$$

Daughter

$$\bar{h}_0^D = 100 \text{ kft} \qquad \bar{\beta}_0^D = 15 \text{ and } 5 \text{ lb/ft}^2$$

with the standard deviations taken as 2 lb/ft^2 on ballistic coefficients, 3 kft on altitudes, and 1 deg on breakoff angles.

Table 2 shows, for the lead edge fragment, a more complete comparison for the improved Allen and Eggers trajectory solution. The velocity and ground range differences are small, while the linear superposition approximation on the flight path angle is in good agreement with the simulation down to an altitude of approximately 60 kft for the 100-β fragment while the 30-β fragment compares well down to approximately 80 kft. Of course, higher-β bodies will show closer comparisons at altitudes below the TBU "modeling region." Table 3 compares the trajectory solutions for a re-entry vehicle having a ballistic coefficient of 1500 lb/ft^2 at two different re-entry angles.

These examples, plus many others, have shown the validity of these analytical models for determining the distribution parameters in that their accuracy is consistent with other TBU modeling assumptions.

Conclusion

In this paper, tank breakup fragment position and velocity joint probability density functions have been derived using analytical partial derivatives based on the Allen and Eggers equations of motion. Comparisons made with realizations generated by a complete Monte Carlo trajectory simulation show the validity of the distributions in the desired modeling region. In cases where greater accuracy is desired for the mean values, the derived covariance matrix can be superimposed upon the mean state computed using a complete trajectory simulation.

The ability to compute fragment distributions is a powerful tool for evaluating fragment clutter effects on ballistic missile defense sensors. Simple but accurate radar clutter models can be realized by processing the fragment distributions through a radar ambiguity function. For example, the video amplitude distribution at the output of a radar quadrature receiver can be derived by performing another transformation of random variables on the fragment position and velocity. The distributions also allow a very accurate calculation of average clutter, since the mathematical expectation can be performed in detail.

Appendix

Primary Fragmentation Intermediate Partials

$$\frac{\partial \bar{h}}{\partial \bar{V}} = \frac{C}{\bar{V}\ln(\bar{K}_0/\bar{V})} \tag{A1}$$

$$\frac{\partial \bar{h}}{\partial \bar{\beta}_0} = \frac{C}{\bar{\beta}_0}\frac{\ln(\bar{V}/\bar{V}_0)}{\ln(\bar{K}_0/\bar{V})} \tag{A2}$$

$$\frac{\partial \bar{h}}{\partial \bar{h}_0} = \frac{\ln(\bar{K}_0/\bar{V}_E)}{\ln(\bar{K}_0/\bar{V})} \tag{A3}$$

$$\frac{\partial h}{\partial \theta}\Big|_{\theta=0} = -\bar{\beta}_0 \cot\gamma_E \frac{\partial \bar{h}}{\partial \bar{\beta}_0} \tag{A4}$$

$$\frac{\partial \bar{m}}{\partial \bar{h}_0} = \frac{1}{\bar{V}_0 \sin\gamma_E} \tag{A5}$$

$$\frac{\partial \bar{f}}{\partial \bar{V}} = -\frac{1}{\bar{V}\sin\gamma_E}\frac{\partial \bar{h}}{\partial \bar{V}} \tag{A6}$$

$$\frac{\partial \bar{f}}{\partial \bar{\beta}_0} = \frac{1}{\bar{\beta}_0}\left[\left(\bar{T}_F - \frac{1}{\sin\gamma_E}\frac{\partial \bar{h}}{\partial \bar{V}}\right)\ln\left(\frac{\bar{K}_0}{\bar{V}_0}\right) + \frac{C}{\bar{\beta}_0}\frac{\partial \bar{m}}{\partial \bar{h}_0}\right] \tag{A7}$$

$$\frac{\partial \bar{f}}{\partial \bar{h}_0} = \frac{\bar{\beta}_0}{C}\left(1 - \frac{\bar{\beta}_0}{\beta_{\rm LE}}\right)\frac{\partial \bar{f}}{\partial \bar{\beta}_0} + \frac{\bar{\beta}_0}{\beta_{\rm LE}}\frac{\partial \bar{m}}{\partial \bar{h}_0} \tag{A8}$$

$$\frac{\partial f}{\partial \theta}\Big|_{\theta=0} = \left(\bar{T}_F - \bar{\beta}_0\frac{\partial \bar{f}}{\partial \bar{\beta}_0}\right)\cot\gamma_E \tag{A9}$$

Secondary Fragmentation Intermediate Partials

$$\frac{\partial \bar{h}}{\partial \bar{V}} = \frac{C}{\bar{V}\ln(\bar{K}_0^D/\bar{V})} \tag{A10}$$

$$\frac{\partial \bar{h}}{\partial \bar{\beta}_0^P} = \frac{C}{\bar{\beta}_0^P}\frac{\ln(\bar{V}_0^D/\bar{V}_0^P)}{\ln(\bar{K}_0^D/\bar{V})} \tag{A11}$$

$$\frac{\partial \bar{h}}{\partial \bar{h}_0^P} = \frac{\ln(\bar{K}_0^P/V_E)}{\ln(\bar{K}_0^D/\bar{V})} \tag{A12}$$

$$\frac{\partial h}{\partial \theta^P}\Big|_{\theta^P=0} = -C\frac{\ln(\bar{V}/\bar{V}_0^P)}{\ln(\bar{K}_0^D/\bar{V})}\cot\gamma_E \tag{A13}$$

$$\frac{\partial \bar{h}}{\partial \bar{\beta}_0^D} = \frac{C\ln(\bar{V}/\bar{V}_0^D)}{\bar{\beta}_0^D\ln(\bar{K}_0^D/\bar{V})} \tag{A14}$$

$$\frac{\partial \bar{h}}{\partial \bar{h}_0^D} = \frac{\ln(\bar{K}_0^D/\bar{K}_0^P)}{\ln(\bar{K}_0^D/\bar{V})} \tag{A15}$$

$$\frac{\partial h}{\partial \theta^D}\Big|_{\theta^D=0} = -\bar{\beta}_0^D\frac{\partial \bar{h}}{\partial \bar{\beta}_0^D}\cot\gamma_E \tag{A16}$$

$$\frac{\partial \bar{m}}{\partial \bar{h}_0^P} = \frac{1}{\bar{V}_0^P \sin\gamma_E} \tag{A17}$$

$$\frac{\partial \bar{f}_1}{\partial \bar{\beta}_0^P} = \frac{1}{\bar{\beta}_0^P}\left[\bar{T}_F^P\ln\left(\frac{\bar{K}_0^P}{\bar{V}_0^P}\right) - \frac{C}{\bar{V}_0^P\sin\gamma_E} + C\frac{\partial \bar{m}}{\partial \bar{h}_0^P}\right] \tag{A18}$$

$$\frac{\partial \bar{f}_2}{\partial \bar{\beta}_0^P} = \frac{1}{\bar{\beta}_0^P}\ln\left(\frac{\bar{V}_0^D}{\bar{V}_0^P}\right)\left(\bar{T}_F^D - \frac{1}{\sin\gamma_E}\frac{\partial \bar{h}}{\partial \bar{V}}\right) \tag{A19}$$

$$\frac{\partial \bar{f}_1}{\partial \bar{h}_0^P} = \frac{\bar{T}^P}{C}\ln\left(\frac{\bar{K}_0^P}{V_E}\right) + \frac{1}{\bar{V}_0^P\sin\gamma_E} \tag{A20}$$

$$\frac{\partial \bar{f}_2}{\partial \bar{h}_0^P} = \frac{1}{C}\ln\left(\frac{\bar{K}_0^P}{V_E}\right)\left(\bar{T}_F^D + \frac{1}{\sin\gamma_E}\frac{\partial \bar{h}}{\partial \bar{V}}\right) \tag{A21}$$

$$\frac{\partial f_1}{\partial \theta^P}\Big|_{\theta^P=0} = \left(\bar{T}_F^P - \bar{\beta}_0^P\frac{\partial \bar{f}_1}{\partial \bar{\beta}_0^P}\right)\cot\gamma_E \tag{A22}$$

$$\frac{\partial f_2}{\partial \theta^P}\Big|_{\theta^P=0} = \frac{\partial f_2}{\partial \theta^D}\Big|_{\theta^D=0} - \bar{\beta}_0^P\frac{\partial \bar{f}_2}{\partial \bar{\beta}_0^P}\cot\gamma_E \tag{A23}$$

$$\frac{\partial \bar{f}_2}{\partial \bar{V}} = -\frac{1}{\bar{V}\sin\gamma_E}\frac{\partial \bar{h}}{\partial \bar{V}} \tag{A24}$$

$$\frac{\partial \bar{f}_2}{\partial \bar{\beta}_0^D} = \frac{1}{\bar{\beta}_0^D}\left[\bar{T}_F^D\ln\left(\frac{\bar{K}_0^D}{\bar{V}_0^D}\right) - \frac{C\ln(\bar{K}_0^D/\bar{V}_0^D)}{\bar{V}\sin\gamma_E\ln(\bar{K}_0^D/\bar{V})} + \frac{C}{\bar{V}_0^D\sin\gamma_E}\right] \tag{A25}$$

$$\frac{\partial \bar{f}_1}{\partial \bar{h}_0^D} = \frac{-1}{\bar{V}_0^D\sin\gamma_E} \tag{A26}$$

$$\frac{\partial \bar{f}_2}{\partial \bar{h}_0^D} = \frac{\bar{T}_F^D}{C}\ln\left(\frac{\bar{K}_0^D}{\bar{K}_0^P}\right) - \frac{\ln(\bar{K}_0^D/\bar{K}_0^P)}{\bar{V}\sin\gamma_E\ln(\bar{K}_0^D/\bar{V})} + \frac{1}{\bar{V}_0^D\sin\gamma_E} \tag{A27}$$

$$\frac{\partial f_2}{\partial \theta^D}\Big|_{\theta^D=0} = \left(\bar{T}_F^D - \bar{\beta}_0^D\frac{\partial \bar{f}_2}{\partial \bar{\beta}_0^D}\right)\cot\gamma_E \tag{A28}$$

Acknowledgment

The work described in this paper was developed for the McDonnell Douglas Astronautics Company-West under Contract DAHC60-72-C-0080. The paper was presented at the AIAA-Cosponsored Booster Tank Breakup – Past, Present, Future Conference, Stanford Research Institite, Menlo Park, Calif., July 26-27, 1977.

References

[1] Allen, H. J. and Eggers, A. J., "A Study of the Motion and Aerodynamic Heating of Ballistic Missiles Entering the Earth's Atmosphere at High Supersonic Speeds," NACA TN4047, Oct. 1957.

[2] Moe, M. M., "An Approximation to the Re-Entry Trajectory," *ARS Journal*, Vol. 30, Jan. 1960, pp. 50-53.

[3] Loh, W.H.T., "A Second-Order Theory of Entry Mechanics into a Planetary Atmosphere," *Journal of the Aerospace Sciences*, Vol. 29, Oct. 1962, pp. 1210-1222.

[4] Loh, W.H.T., "Some Exact Analytical Solutions of Planetary Entry," *AIAA Journal*, Vol. 1, April 1963, pp. 836-842.

[5] Loh, W.H.T., *Dynamics and Thermodynamics of Planetary Entry*, Prentice-Hall, Inc., Englewood Cliffs, N. J., 1963.

[6] Citron, S. J. and Meir, T. C., "An Analytic Solution for Entry into Planetary Atmospheres," *AIAA Journal*, Vol. 3, March 1965, pp. 470-475.

[7] Wolverton, R. W. (ed.), *Flight Performance Handbook for Orbital Operations*, John Wiley and Sons, Inc., N. Y., 1963, Sec. 6.4.2.

[8] Morris, D. N. and Benson, P., "Data for ICBM Re-Entry Trajectories," The Rand Corp., Santa Monica, Calif., RM-3475-ARPA, April 1963.